Dynamical regimes and transitions in Plio-Pleistocene Asian monsoon

2012 EPL 97 40009

(http://iopscience.iop.org/0295-5075/97/4/40009)

A Letters Journal Exploring the Frontiers of Physics

February 2012

EPL, **97** (2012) 40009
doi: 10.1209/0295-5075/97/40009

www.epljournal.org

Dynamical regimes and transitions in Plio-Pleistocene Asian monsoon

N. Malik[1,2,3(a)], Y. Zou[2,4,5], N. Marwan[2] and J. Kurths[2,6]

[1] *Department of Mathematics, CB#3250, University of North Carolina - Chapel Hill, NC 27599, USA*
[2] *Potsdam Institute for Climate Impact Research - P.O. Box 601203, 14412 Potsdam, Germany, EU*
[3] *Institute of Physics, University of Potsdam - Karl-Liebknecht-Str. 24/25, 14476 Potsdam-Golm, Germany, EU*
[4] *Department of Physics, East China Normal University - Shanghai 200241, China*
[5] *Department of Electronic and Information Engineering, The Hong Kong Polytechnic University Hunghom Kowloon, Hong Kong*
[6] *Department of Physics, Humboldt University Berlin - Newtonstr. 15, 12489 Berlin, Germany, EU*

received 7 October 2011; accepted in final form 20 January 2012
published online 22 February 2012

PACS 05.10.-a – Computational methods in statistical physics and nonlinear dynamics
PACS 05.45.Tp – Time series analysis
PACS 92.60.Iv – Paleoclimatology

Abstract – We propose a novel approach based on the *fluctuation of similarity* to identify regimes of distinct dynamical complexity in short time series. A statistical test is developed to estimate the significance of the identified transitions. Our method is verified by uncovering bifurcation structures in several paradigmatic models, providing more complex transitions compared with traditional Lyapunov exponents. In a real-world situation, we apply this method to identify millennial-scale dynamical transitions in Plio-Pleistocene proxy records of the South Asian summer monsoon system. We infer that many of these transitions are induced by the external forcing of the solar insolation and are also affected by internal forcing on Monsoonal dynamics, *i.e.*, the glaciation cycles of the Northern Hemisphere and the onset of the Walker circulation.

Introduction. – Detecting points of changes of dynamical complexity is of considerable interest in a wide variety of fields [1], like finance (detecting stock market crashes), life sciences (identifying pathological activities of heart attacks or epileptic seizures [2]), paleoclimate (uncovering tipping points in the climate system [3]) or physics (studying the response of interacting many-body system to an external perturbation [4]). Dynamical transitions could be due to different dynamics when the control parameter passes bifurcation thresholds; internal slow drifting of some parameter with dynamics qualitatively unchanged; the system experiences abrupt changes under external forceful influences; parameter variation of the external forcing; or noise effects as well. One of the geophysical analogies to such situations is solar forcing which acts as the main external driver for the evolution of Earth's climate on different time scales. The variation of parameters might not always lead to extreme changes in the dynamics but could also lead to some subtle changes which are very hard to detect either by mere visual inspection or by linear time series analysis methods.

Among many geophysical processes, a highly practical problem is to identify major dynamical transitions that have occurred in the Asian monsoonal system and to obtain clues about the processes and events that causes these transitions. This is important because the monsoons are among the most critical climatic phenomena manifesting in the tropics with far reaching societal impacts. Their study at palaeo time scales is of enormous interest for the understanding of the global climate system and its evolution. We here study the dynamical evolution of the Asian monsoonal system at millennial time scales and find that major dynamical shifts in it are driven by the changes in the solar insolation and the Northern Hemisphere (NH) glaciation cycles [5].

Since many geophysical processes are nonstationary and only short time series are available due to technical measurement restrictions, we propose here a rather simple yet robust method to detect dynamical transitions in short time series. This task becomes even more challenging when mutually interacting processes are responsible

(a) E-mail: malik@pik-potsdam.de

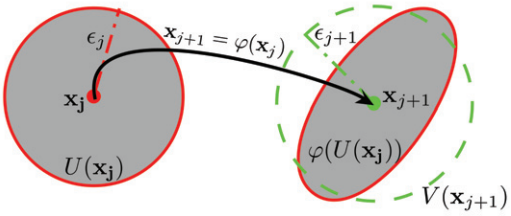

Fig. 1: (Color online) Schematic representation of the ϵ_j ball neighbourhood $U(\mathbf{x}_j)$ of the time point $\mathbf{x}_j$ corresponding to k-closest neighbours of $\mathbf{x}_j$ and its deformation into an ellipsoid due to the application of mapping φ on it in a case of $\mathbf{x}_{j+1} = \varphi(\mathbf{x}_j)$ (see grey region within the red boundary). The neighbourhood of $\mathbf{x}_{j+1}$ corresponding to its k-nearest neighbours is usually different and it is shown with the green boundary $V(\mathbf{x}_{j+1})$.

for the dynamical transitions and hardly being distinguished. Most of the existing nonlinear methods proposed in the literature in dealing with nonstationary time series are mainly based on recurrences [6–8] or recurrence time statistics [9] of the underlying system. These methods are often either context dependent (*e.g.*, epileptic seizure detection in EEG data [7]) or require very long time series [9], which is practically often unlikely and unavailable. In this letter, we propose a new method to identify dynamical transitions in a short univariate time series. A measure of similarity is introduced to distinguish two points of similar dynamics from two time points of different dynamics. Our method hinges on the concept of nonlinear interdependency which was proposed for extracting coupling direction for bivariate time series [10]. Instead of measuring the interdependence between two different time series, we quantify the *fluctuation of similarity* between states at two time points, which takes into account the information contained in the entire single time series.

Method. – The concept of *similarity* here is defined in terms of the conditional closeness of one point to the neighbourhood of another point. Let $\mathbf{x}_j$ represent the j-th vector of a delay embedded time series with length N. The embedding dimension m and time delay L are suggested respectively by fixed nearest neighbours and mutual information (cf. [11]). In the phase space we denote the neighbourhood of any point $\mathbf{x}_j$ as $U(\mathbf{x}_j)$ containing k number of closest neighbours of $\mathbf{x}_j$, namely $U(\mathbf{x}_j) = \{\mathbf{x}_l : \|\mathbf{x}_l - \mathbf{x}_j\| < \epsilon_j\}$, where $l \in \{l_1, l_2, \ldots, l_k\}$, and $\|\cdot\|$ is a norm. For each point $\mathbf{x}_j$, ϵ_j is chosen in such a way that k remain constant over the series. The requirement of the method is that k must be substantially smaller than N. In all the examples and application below we have taken 5% of points as k closest neighbours. The pointwise *closeness* of $\mathbf{x}_j$ to its k neighbours is obtained as the mean distance $d(\mathbf{x}_j) = \frac{1}{k}\sum_{l=l_1}^{l_k} \|\mathbf{x}_j - \mathbf{x}_l\|$. After some time evolution τ at time $j+\tau$, the k closest neighbourhood of $\mathbf{x}_{j+\tau}$ is generally different and is given by $V(\mathbf{x}_{j+\tau}) = \{\mathbf{x}_i : \|\mathbf{x}_i - \mathbf{x}_{j+\tau}\| < \epsilon_{j+\tau}\}$, where $i \in \{i_1, i_2, \ldots, i_k\}$. In fig. 1 we show a schematic representation of these neighbourhoods and their evolution for two consecutive time points. The *conditional closeness* of $\mathbf{x}_{j+\tau}$ to the neighbourhood of $\mathbf{x}_j$ is calculated in a similar way by the mean distance as $d(\mathbf{x}_{j+\tau}|\mathbf{x}_j) = \frac{1}{k}\sum_{l=l_1}^{l_k} \|\mathbf{x}_{j+\tau} - \mathbf{x}_l\|$. Thus, the *similarity* of $\mathbf{x}_j$ to $\mathbf{x}_{j+\tau}$ is defined by the ratio of closeness and conditional closeness as

$$S_{j|j+\tau} = \frac{d(\mathbf{x}_j)}{d(\mathbf{x}_{j+\tau}|\mathbf{x}_j)}. \tag{1}$$

In a full analogy, $S_{j+\tau|j}$ characterising the similarity of $\mathbf{x}_{j+\tau}$ conditioned to $\mathbf{x}_j$ can be calculated, which often yields $S_{j|j+\tau} \neq S_{j+\tau|j}$ since $d(\mathbf{x}_{j+\tau}|\mathbf{x}_j) \neq d(\mathbf{x}_j|\mathbf{x}_{j+\tau})$. Larger values of $S_{j|j+\tau}$ indicate higher similarities in the signal. It is easy to see that $S_{j|j+\tau}$ is also time dependent, for, *e.g.*, a periodic trajectory with period T, $\mathbf{x}_j = \mathbf{x}_{j+nT}$ yields a periodic variation of $S_{j|j+\tau}$. With varying the index τ, $S_{j|j+\tau}$ acts as a nonlinear autocorrelation function.

To identify dynamical transitions we propose to characterise changes of similarity between the recurrence structures of two consecutive time points *i.e.*, we fix $\tau = 1$. If no dynamical transition has occurred at j, then there will exist a smooth mapping φ such that $\mathbf{x}_{j+1} = \varphi(\mathbf{x}_j)$ for all j, in such a case for a finite time series $S_{j|j+1}$ is expected to fluctuate close to a constant value specific to a φ. Else, if dynamical transition has occurred at j then it would invariably lead to break down of determinism *i.e.*, there will exist no such φ. This in turn will lead to substantially large and sharp fluctuations in $S_{j|j+1}$. To quantify these fluctuations and to identify dynamical transition we introduce the *fluctuation of similarity* σ_S as the variance of $S_{j|j+1}$,

$$\sigma_S^2 = \langle (S_{j|j+1} - \mu_S)^2 \rangle, \tag{2}$$

where $\mu_S = \langle S_{j|j+1} \rangle$, and $\langle\cdot\rangle$ denote an average over N points. σ_S has been found to be sensitive to the abrupt dynamical transitions in a time series. Therefore, a point of sharp change in σ_S, combined with a statistical significance test of this change will indicate a dynamical transition. Further, it can also be analytically proven that σ_S is related with dynamical complexity of the underlying system. This proof will be provided in a forthcoming paper.

Numerical examples and significance test. – As a numerical example in support of σ_S dependence on dynamical complexity in a time series, we choose to analyse dynamical transitions in the Logistic map $x_{n+1} = rx_n(1-x_n)$ with a varying control parameter r from 3.5 to 4 with step size 0.0005. We consider time series of 1000 points at each value of r (after removing 500 transient points). In fig. 2 we observe that there is baseline of σ_S, it falls below only for lowest complexity dynamics (periodic windows). Also, for higher complexity chaotic dynamics σ_S exhibit larger values. σ_S clearly indicates even more subtle transitions (*i.e.* chaos-to-chaos, for, *e.g.*, laminar phases), which are not identified by λ.

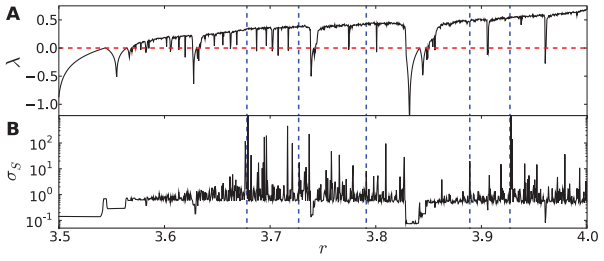

Fig. 2: (Color online) Analysis of the Logistic map. (A) Lyapunov exponent λ, (B) σ_S. Several vertical dashed lines ($r = 3.678$, 3.727, 3.791, 3.889, 3.927) highlight some chaos-to-chaos transitions with laminar phases, which agree well with the results provided by the super-track function [8,12].

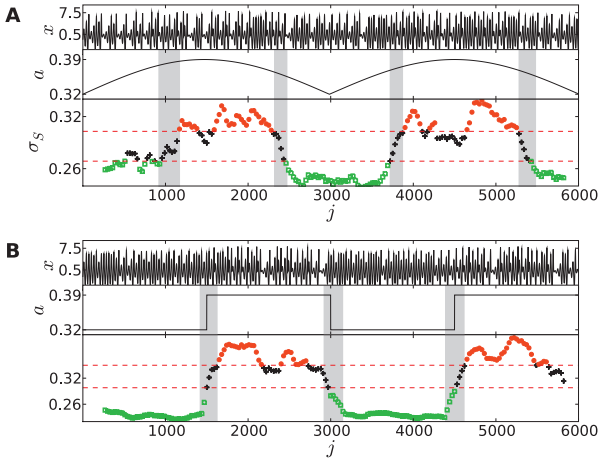

Fig. 3: (Color online) Transition between spiral- and screw-type chaos in the Rössler system (see footnote [1]). (A) Slow nonlinear approaching to transition points. (B) Abrupt transitions. Time series of the x-component are shown in the upper panels of both (A) and (B), middle panels show the variation of a, lower panels are σ_S. Horizontal dashed lines in the lower panels of both (A) and (B) are 90% confidence bounds. The values of σ_S above and below the band are colored in orange (dots) and green (open squares), respectively, and black (plus signs) if they lie inside the band. This is done to highlight the regimes of two distinct dynamical complexities. Note that the crossover of the significance levels happens only around the points of dynamical transition (highlighted by vertical grey bands).

We next apply the method to more realistic situations where we have a short time series (of length N) obtained from a dynamical system whose parameters vary in a certain way with time. In all the numerical studies below, we use the same procedure as follows: First we calculate $S_{j|j+1}$ for all the j points in the series, then σ_S is computed with sliding windows of size n. The temporal profile of σ_S is therefore used to disclose possible hidden transitions of complexity changes. We apply a bootstrapping method [13] to test the null hypothesis that the similarity measure represented by $S_{j|j+1}$ is uniform for the original process. We create the null model by randomly drawing n values with replacement from the series of $S_{j|j+1}$, where n is the window size. By repeating this procedure many times (*e.g.*, 10000 times throughout the paper), we construct an ensemble of σ_S^i. The 0.05 and 0.95 percent quantiles of this ensemble could be interpreted as 90% confidence bounds. The points below and above the significance band are less likely to happen, hence we can classify these points as belonging to dynamics of two distinct complexity with 90% confidence. The time band over which the *crossover between the two levels* occurs contain the point of dynamical transition. The points with lower values of σ_S could be regarded as belonging to the dynamical regimes which are relatively more stable.

As a paradigmatic example, we use the Rössler model[1]. The system shows two distinct chaotic attractors when increasing the parameter a from 0.32 to 0.39, respectively corresponding to the spiral and screw type chaos. The transition between both chaotic regimes is due to the formation of a homoclinic orbit [14]. In the first case we implement a transient variation of the control parameter a by $a(t) = 0.32 + 0.07|\sin(\frac{\pi}{600}t)|$ at each integration step, where t is the step size for the fourth order Runge-Kutta integrator ($t = 0.001$). The sampling time between two consecutive points is $\delta t = 0.2$ and we use 6000 points of the x-component (see footnote [1]) (fig. 3). In the case of nonstationarity (*i.e.*, due to time varying parameter a), overembedding techniques are necessary and widely used as it was suggested that $m > 2D + p$, where D is the dimension of the attractor and p is the number of varying parameters [15]. Therefore we choose the embedding parameters $m = 10$ and $L = 15$. We calculate σ_S by sliding window of size $n = 300$ and 90% overlapping between two windows based on the similarity series of $S_{j|j+1}$. σ_S varies significantly from lower to higher values and vice versa (highlighted by grey bands in fig. 3(A)), which indicate slow changes in the complexity of dynamics between the two distinct chaotic states.

In the next case, the parameter a switches between 0.32 and 0.39 after 1500 sampled points, yielding abrupt transitions from one dynamical complexity to the other. The other parameters for calculating σ_S are the same as in the previous case. Convincingly, σ_S captures the abrupt transitions very clearly (fig. 3(B)). It is important to emphasise that our method works analogously i) in the presence of noise, and ii) in the case in which we introduce missing values in the time series to mimic the situation we have in the palaeo records used below. At this point we presume that statistically distinct values of σ_S correspond to distinct dynamics in a system evolving with time. A time span over which the crossover from the values below the significance band to above the significance occurs, highlights the time of occurrence of dynamical transitions (shown as grey vertical bars in fig. 3). Next we will apply this procedure to an observational time series to identify possible transition points.

[1]Rössler model: $\dot{x} = -y - z$, $\dot{y} = x + ay$, $\dot{z} = 0.3x - 4.5z + xz$.

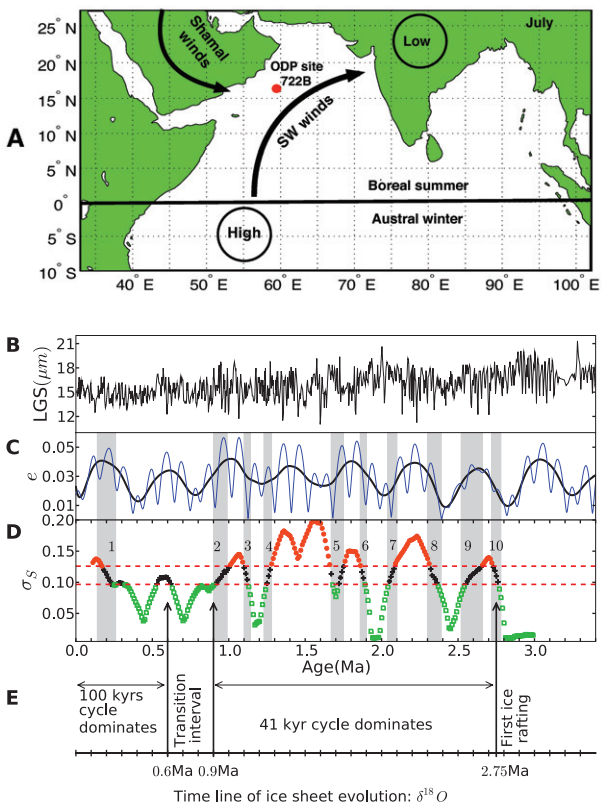

Fig. 4: (Color online) (A) Map of winds in July from high pressure in the Indian Ocean to low pressure over the land. The bullet dot denotes the location of the ODP site 722B (16°37′N, 59°48′E, 2028 meters below the sea level). (B) LGS time series. (C) The blue line is the orbital eccentricity e and the dark bold line is the associated 400 kyr component. (D) σ_S. The 90% confidence bound is represented by horizontal dashed lines. Orange (dots) and green (open squares) separate the regimes of two different dynamical complexity. (E) Time line of the NH glaciation as reconstructed from δ^{18}O record [16]. Vertical arrows indicate the important events in the ice history, which are adapted from [17]. See the text for details of bands in (C), (D).

Application. – One of the most important monsoonal system on the Earth is the South Asian summer monsoon which affects the life of billions of inhabitants of the region. Its origin lies in the temperature gradient between the land and the sea that ceases to exist during the peak of summer, which, in turn, leads to a pressure difference between the land and the sea resulting in strong moisture laden winds blowing from the high pressure areas of the sea to the low pressure areas of the land (see fig. 4(A)). The lithogenic grain size (LGS) in marine sediments is an ideal proxy for the *wind* intensity (carrying capacity) over geological time scales which can be used for studying the variability of the monsoon in the past. One of the longest records for the Asian monsoon is a LGS record from the Ocean Drilling Program (ODP) site 722B extending for the last 3.41 million years (Ma) before present [5]. It has a sampling rate of 0.001 Ma but with a large number of missing values in the series [5] (fig. 4(B)). δ^{18}O is one of the best proxies reflecting global surface *temperature*, serving as an indicator of the global ice volume variability [16] (fig. 4(E)). Based on the information provided by δ^{18}O record, we have marked the important events in the glaciation time line of NH by vertical arrows in fig. 4(D), (E). The δ^{18}O data used here, is from ref. [18].

To get over the problem of missing values in LGS data set, we replace the missing values with flags (*e.g.*, large number 9999) which act as place holders. The time series was normalised to zero mean and unit variance before placing the flags. As LGS is a proxy of a physical process with high dimensions and large parameter space, we embed the time series in a high dimensional space by taking embedding parameters $m = 30$ and $L = 5$, *i.e.*, a vector in embedded space spans 0.15 Ma. Such a high dimensional space (in a range of 15 ∼30) was suggested to minimise the possible effects of both nonstationarity and noise present in time series [15]. Based on $S_{j|j+1}$, we used a window size of $n = 100$ (0.1 Ma) with 90% of overlapping. We present a 90% confidence bound as estimated by bootstrapping. The values of σ_S above and below the significance band separate out two distinct dynamical regimes. The time points where crossing of significance band takes place are the points where dynamical transitions have occurred. In the parlance of palaeoclimatic terminology, the values of σ_S for the LGS data set could be interpreted as patterns of palaeoclimatic variability of the South Asian monsoonal system on the orbital time scales. The transitions identified by σ_S are highlighted by grey bands in fig. 4(D) and summarised in table 1, which also shows a comparison to the results reported by linear time series methods in the literature on similar data sets.

The main external forcing at the orbital time scales (10^6 years) on the South Asian monsoonal system is the change in the solar insolation induced by the cyclic variability of orbital parameters of Earth. Internally, the evolution of monsoon has also been effected by changes in the Northern Hemisphere (NH) ice sheets and the sea surface temperatures [19]. The dominant factor in the astrodynamical calculations of the insolation received by the Earth is $e\sin(\beta)$, where e is the eccentricity and β is the precession [20]. The high number of missing values and low temporal resolution (>0.001 Ma) of LGS data set do not allow us to study the influences of the higher frequency variation of solar insolation on monsoon. Therefore, we have concentrated on comparing the dynamical changes and transitions that have occurred in the monsoon over the time scales of cyclicity in eccentricity of Earth's orbit (400 kyr and 100 kyr). In the original analysis of [5] (besides LGS data), the authors concentrated on coherence between the monsoonal variability and the insolation forcing associated with the obliquity and precession bands. The relations to the eccentricity has not been discussed seriously, since their methods generally could not yield interpretable results, which they hence argued the direct insolation forcing associated with eccentricity is negligible

Table 1: Comparison of transitions identified by σ_S and by other approaches reported for similar data sets. Time unit is Ma.

Band's index	1	2	3	4	5	6	7	8	9	10
σ_S on LGS	0.14–0.27	0.9–1.0	1.1–1.15	1.23–1.28	1.67–1.75	1.86–1.91	2.04–2.1	2.3–2.39	2.52–2.67	2.72–2.79
Ref. [5] on LGS	–	–	–	∼1.2	∼1.7	–	–	–	∼2.6	–
Ref. [21] on Dust flux	–	∼1.0	–	–	∼1.7	–	–	–	–	∼2.8

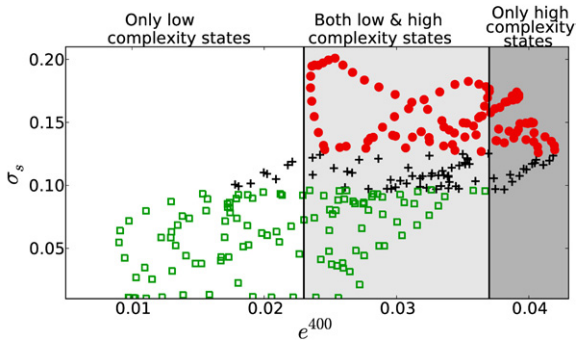

Fig. 5: (Color online) Scatter plot between σ_S and e^{400} (400 kyr cycle of eccentricity). Green (open squares), black (plus) and orange (dots) points are the same as in fig. 4 and represent the low complexity dynamics, the statistically insignificant values and the high complexity dynamics, respectively.

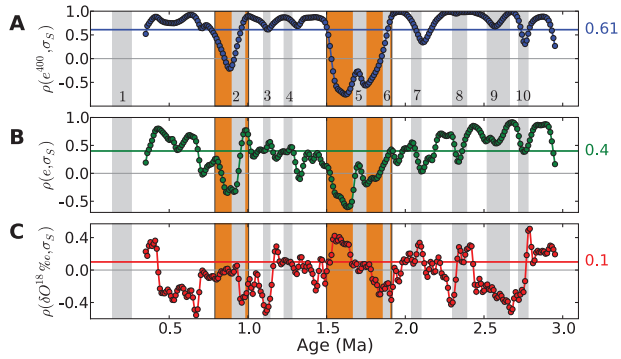

Fig. 6: (Color online) Windowed correlation: the cross-correlation between σ_S and e^{400} (A), e (B) and δ^{18}O record (‰) (C). The correlation coefficient ρ is calculated over 25 points using a 99% overlap. The horizontal colored lines correspond to cross-correlation for each indicated parameter over the whole series. The values are quoted in the same color on the right-hand side. The two vertical orange bands indicate a sharp drop in $\rho(e^{400}, \sigma_S)$ and $\rho(e, \sigma_S)$. Grey bands are the same as in fig. 4. Transitions 3, 7, 8, 10 also show sharp changes in $\rho(e, \delta^{18}\text{O})$.

for understanding monsoon strength. As a matter of fact, the orbital eccentricity e characterises the lowest frequency variation of the solar cycle, modulating the precession on two different time scales, 100 kyr and 400 kyr, which have been observed in many palaeoclimate data sets, *e.g.*, dust flux records [21,22]. It has been noted in [23] that the highest palaeoclimatic variability in ODP records from the region occurs during the periods of maximum orbital eccentricity e. We show e by thin blue line in fig. 4(C) together with its 400 kyr component as a dark bold line, represented by the notation e^{400} in the text. Because of the length and resolution of the available LGS data, we compare the transitions captured by σ_S to the variabilities of both the 400 kyr cycle and glaciation of the NH (fig. 4(C), (E), respectively).

Discussion. – From fig. 4(D) and table 1, we find that most of the transitions identified essentially show the basic response mechanism of the monsoonal system to the external solar forcing, with some exceptions. The response behaviour is captured by the measure of σ_S, which reveals a strong relationship with the 400 kyr component of the eccentricity e. Higher values of e lead to higher values of σ_S and lower values of e imply lower values of σ_S, indicating σ_S varying between two different phases of dynamical complexity (or relative dynamical stability). In fig. 5 we observe a kind of threshold behaviour of monsoon dynamics (σ_S) with respect to changes in e^{400}. No point of high complexity (dots) is observed for $e^{400} < 0.023$. Similarly no point of low complexity (open squares) is observed for $e^{400} > 0.037$. Which hints towards that higher complexity (or lower stability) in the monsoon dynamics tends to occur during the high insolation periods. In the range $0.023 < e^{400} < 0.037$, it is seen that both kinds of dynamical regimes are possible and in this range we think that the higher frequency variation of solar insolation and internal feedbacks of monsoonal system must be important in determining the complexity of the dynamical regime.

We observe in fig. 4(D) that mostly low complexity points (open squares) occurred before 1.0 Ma. The response to solar insolation is subdued in this time slice as reflected by small variation of σ_S compared to other parts of its variation in the series. This is the period of glaciation in NH and most parts of the Earth were cooler than modern state [16,17,24]. This indicates towards a possible important role played by NH ice sheet evolution on the evolution of modern summer monsoon over South Asia. Furthermore, we notice two other important transitions which are denoted by bands-4 (∼1.2) and 10 (∼2.75). The former was supported by the transition of the ice cycles [5], while the latter one corresponds to time point when the first ice sheet appeared in the NH. After 1.2 Ma relatively large deviations were observed in σ_S. This was the period of development of strong Walker circulation and after 2.0 Ma low- and mid-latitude regions of Earth were warmer than the modern state, hinting the plausibility of stronger variation in the monsoon dynamics in warmer environments.

To further solidify our analysis in fig. 6 we have studied the windowed cross-correlation ρ between σ_S and the other three parameters *viz.*, e^{400} (400 kyr cycle of e), e (the full e *i.e.*, 100 kyr cycle) and δ^{18}O. In fig. 6(A), (B) we observe high positive correlations between σ_S and e^{400} and also between σ_S and e. This suggests that the dynamical

complexity of the monsoon responds in an almost linear way to the changes of the solar insolation. The relationship between σ_S and e suggests that the solar insolation acts as an external varying forcing parameter for the South Asian summer monsoon system, where slight variations induce large changes in the dynamical complexity of the monsoon. Also, we observe two very sharp fluctuations in $\rho(e^{400}, \sigma_S)$ and $\rho(e, \sigma_S)$ (orange vertical bands in fig. 6), where these ρ simultaneously change sign. One of such a transition occurred around 0.8–1.0 Ma, where $\rho(e^{400}, \sigma_S)$ and $\rho(e, \sigma_S)$ have values very close to zero. This means that the dynamical responses of monsoon became independent of solar forcing during this period. A plausible cause for the emergence of such a feature could be the known fact that this was the period of transition in the cyclicality in NH ice sheets [16]. The variation in NH ice sheet could modulate monsoon via the changes in patterns of planetary albedo. The other transition happened around 1.5–1.9 Ma (see orange band in fig. 6). Here the values of $\rho(e^{400}, \sigma_S)$ and $\rho(e, \sigma_S)$ become large negative, implying that monsoon dynamics responded in characteristically opposite way to its usual response to solar forcing and its variations. A possible reason could be the development of strong Walker circulation during this period [24]. The influence of the intensification of Walker circulation could come via the changing sea surface temperature. All these exceptions suggest that major changes in internal forcing of the climate system like glaciation cycles and oceanic circulations could significantly disturb the basic response mechanism of the monsoon to the solar insolation. We observe in fig. 6(C) that correlation between the NH ice cover (δ^{18}O record) and monsoon dynamics (σ_S) is rather weak and with some sharp rises and drops to higher positive and negative correlations corresponding to identified transition bands 3, 7, 8 and 10. This indicates that the influence of the NH ice cover on the monsoon dynamics is more episodic, *i.e.*, there are a few events when we observe changes in NH ice cover influencing monsoon dynamics in some way.

Conclusion. – In summary, we propose a new approach, namely the fluctuation of similarity, for identifying transitions between regimes of distinct dynamical complexity in a short time series. Additionally we provide an application of the method to a palaeo-pleistocene record of the Asian monsoonal system. Our results suggest that complexity in the dynamics of South Asian summer monsoon has a linear dependence on the variations in solar insolation due to changes in orbital parameters. The existence of a 400 kyr cycle is very apparent in the LGS data set analysed. Episodic influences of changes in the NH ice sheets and oceanic circulations have also been observed. We stress that our method has broad applications for a general purpose as we have demonstrated by both several prototypical model systems and experimental time series.

* * *

This work was supported by the projects: DFG(GK1364) and HIMPAC. YZ is supported by the Hong Kong Polytechnic University Postdoctoral Fellowship.

REFERENCES

[1] Scheffer M., *Critical Transitions in Nature and Society* (Princeton University Press) 2009.
[2] Lehnertz K. and Elger C. E., *Phys. Rev. Lett.*, **80** (1998) 5019.
[3] Lenton T. M., Held H., Kriegler E., Hall J. W., Lucht W., Rahmstorf S. and Schellnhuber H. J., *Prac. Natl. Acad. Sci. U.S.A.*, **105** (2008) 1786.
[4] Chakrabarti B. K. and Acharyya M., *Rev. Mod. Phys.*, **71** (1999) 847.
[5] Clemens S. C., Murray D. W. and Prell W. L., *Science*, **274** (1996) 943.
[6] Schreiber T., *Phys. Rev. Lett.*, **78** (1997) 843.
[7] Rieke C., Sternickel K., Andrzejak R. G., Elger C. E., David P. and Lehnertz K., *Phys. Rev. Lett.*, **88** (2002) 244102.
[8] Marwan N., Donges J. F., Zou Y., Donner R. V. and Kurths J., *Phys. Lett. A*, **373** (2009) 4246; Marwan N., Romano M., Thiel M. and Kurths J., *Phys. Rep.*, **438** (2007) 237.
[9] Gao J. B., *Phys. Rev. Lett.*, **83** (1999) 3178.
[10] Arnhold J., Grassberger P., Lehnertz K. and Elger C., *Physica D*, **134** (1999) 419.
[11] Kantz H. and Schreiber T., *Nonlinear Time Series Analysis*, 2nd edition (Cambridge University Press, Cambridge) 2004.
[12] Oblow E. M., *Phys. Lett. A*, **128** (1988) 406.
[13] Palus M., *Phys. Rev. Lett.*, **101** (2008) 134101.
[14] Gaspard P. and Nicolis G., *J. Stat. Phys.*, **31** (1983) 499.
[15] Hegger R., Kantz H., Matassini L. and Schreiber T., *Phys. Rev. Lett.*, **84** (2000) 4092.
[16] Raymo M., *Annu. Rev. Earth Planet. Sci.*, **22** (1994) 353.
[17] Ruddiam W. F., *Earth's Climate Past and Future* (W. H. Freeman Company) 2008.
[18] Tiedemann R., Sarnthein M. and Shackleton N. J., *Paleoceanography*, **9** (1994) 619.
[19] Clemens S., Prell W., Murray D., Shimmield G. and Weedon G., *Nature*, **353** (1991) 1991; Pausata F. S. R., Battisti D. S., Nisancioglu K. H. and Bitz C. M., *Nat. Geosci.*, **4** (2011) 474.
[20] Laskar J., Gastineau M., Joutel F., Robutel P., Levrard B. and Correria A., *Astron. Astrophys.*, **428** (2004) 261.
[21] deMenocal P. B., *Science*, **270** (1995) 53.
[22] Trauth M. H., Larrsoaña J. C. and Mudelsee M., *Quat. Sci. Rev.*, **28** (2009) 399.
[23] deMenocal P. B., *Earth Planet. Sci. Lett.*, **220** (2004) 3.
[24] Ravelo A. C., *Oceanography*, **19** (2006) 114.